



Contents lists available at ScienceDirect

## Bioorganic &amp; Medicinal Chemistry Letters

journal homepage: [www.elsevier.com/locate/bmcl](http://www.elsevier.com/locate/bmcl)

## Synthesis and biological evaluation of novel F-18 labeled pyrazolo[1,5-*a*]pyrimidine derivatives: Potential PET imaging agents for tumor detection

Jingli Xu<sup>a</sup>, Hang Liu<sup>a</sup>, Guixia Li<sup>a</sup>, Yong He<sup>a</sup>, Rui Ding<sup>a</sup>, Xiao Wang<sup>a</sup>, Man Feng<sup>a</sup>, Shuting Zhang<sup>a</sup>, Yurong Chen<sup>a</sup>, Shilei Li<sup>a</sup>, Mingxia Zhao<sup>a</sup>, Chuanmin Qi<sup>a,\*</sup>, Yonghong Dang<sup>b</sup>

<sup>a</sup> Key Laboratory of Radiopharmaceuticals (Beijing Normal University), Ministry of Education, College of Chemistry, Beijing Normal University, Beijing 100875, China

<sup>b</sup> Department of Nuclear Medicine, PUMC Hospital, Beijing 100730, China

## ARTICLE INFO

## Article history:

Received 12 February 2011

Revised 3 June 2011

Accepted 16 June 2011

Available online 23 June 2011

## Keywords:

F-18 labeled

Pyrazolo[1,5-*a*]pyrimidine derivatives

PET imaging agents

Tumor detection

## ABSTRACT

Two novel pyrazolo[1,5-*a*]pyrimidine derivatives, 7-(2-[<sup>18</sup>F]fluoroethylamino)-5-methylpyrazolo[1,5-*a*]pyrimidine-3-carbonitrile ([<sup>18</sup>F]FEMPPC, [<sup>18</sup>F]1) and *N*-(2-(3-cyano-5-methylpyrazolo[1,5-*a*]pyrimidin-7-ylamino)ethyl)-2-[<sup>18</sup>F]fluoro-4-nitrobenzamide ([<sup>18</sup>F]FCMPPN, [<sup>18</sup>F]2), have been designed and successively labeled with <sup>18</sup>F by the nucleophilic substitution employing tosylate and nitril as leaving groups, respectively. The radiochemical synthesis of both compounds was completed within 60 min with final high-performance liquid chromatography purification included. The corresponding radiochemical yields (without decay correction) were approximately 35% and 30%, respectively. Meanwhile, we compared the uptake characteristics of [<sup>18</sup>F]1 and [<sup>18</sup>F]2 with those of [<sup>18</sup>F]FDG and L-[<sup>18</sup>F]FET in S180 tumor cells. Furthermore, the tumor uptake of [<sup>18</sup>F]1 and [<sup>18</sup>F]2 was assessed in mice bearing S180 tumor and compared with [<sup>18</sup>F]FDG and L-[<sup>18</sup>F]FET in the same animal model. In vitro cell uptake studies showed [<sup>18</sup>F]1 had higher uptake than [<sup>18</sup>F]FDG, [<sup>18</sup>F]2 and L-[<sup>18</sup>F]FET over the 2 h period. In ex vivo biodistribution showed tumor/brain uptake ratios of [<sup>18</sup>F]2 were 12.35, 10.44, 8.69 and 5.13 at 15 min, 30 min, 60 min and 120 min post-injection, much higher than those of L-[<sup>18</sup>F]FET (2.43, 2.54, 2.93 and 2.95) and [<sup>18</sup>F]FDG (0.59, 0.61, 1.02 and 1.33) at the same time point. What's more, the uptake of [<sup>18</sup>F]1 in tumor was 1.88, 4.37, 5.51, 2.95 and 2.88 at 5 min, 15 min, 30 min, 60 min and 120 min post-injection, respectively. There was a remarkable increasing trend before 30 min. The same trend was present for L-[<sup>18</sup>F]FET before 30 min and [<sup>18</sup>F]FDG before 60 min. Additionally, the tumor/brain uptake ratios of [<sup>18</sup>F]1 were superior to those of [<sup>18</sup>F]FDG at all the selected time points, the tumor/muscle and tumor/blood uptake ratios of [<sup>18</sup>F]1 at 30 min were higher than those of L-[<sup>18</sup>F]FET at the same time point. MicroPET image of [<sup>18</sup>F]1 administered into S180 tumor-bearing mouse acquired at 30 min post-injection illustrated that the uptake in S180 tumor was obvious. These results suggest that compound [<sup>18</sup>F]1 could be a new probe for PET tumor imaging.

© 2011 Elsevier Ltd. All rights reserved.

Pyrazolopyrimidines have multiple pharmacological activities including hypnotic,<sup>1</sup> anti-inflammatory,<sup>2</sup> anti-tumor,<sup>3–7</sup> antimycobacterial<sup>8</sup> and anti-viral.<sup>9,10</sup> Owing to the similarity in structure to purine, pyrazolo[1,5-*a*]pyrimidine and its derivatives have attracted broad interest for the years.<sup>11</sup> They were found to have antitrypanosomal<sup>12</sup> and antischistosomal activity,<sup>13</sup> and most importantly, anti-tumor activity.<sup>14–17</sup> It has been found that many pyrazolo[1,5-*a*]pyrimidine derivatives may block proliferation of various cancer cell lines.<sup>15,18,19</sup> As a result, pyrazolo[1,5-*a*]pyrimidine was widely applied as an important pharmacophore or building block in anti-tumor drug design, which was motivating further study on physiological and biological property of this kind

of compounds, including in vitro stability, in vivo distribution, metabolism and elimination. With the increasing availability of PET (positron emission topography) to provide quantitative kinetic information of metabolic pathways and physiological processes in vivo,<sup>20</sup> PET and in particular integrated PET/CT technique can detect diseases earlier and more accurately than any other imaging technique. A PET/CT is an effective tool to help stage local, regional, distant disease and provide therapeutic guidance for cancer therapy. Of all the most commonly used positron emission isotopes, <sup>18</sup>F is the most favorable mainly due to its longer physical half-life of 110 min,<sup>21</sup> the comparable size to H atom and lower positron energy. 2-[<sup>18</sup>F]fluoro-2-deoxyglucose (<sup>18</sup>F-FDG), an analog of glucose, is the most widely used compound for cancer detection.<sup>22</sup> In spite of being a very effective PET tracer for many types of tumors, <sup>18</sup>F-FDG can suffer from certain limitations: because high

\* Corresponding author.

E-mail address: [qicmin@sohu.com](mailto:qicmin@sohu.com) (C. Qi).

accumulation in inflammation and infection can lead to false-positive results and low uptake in tumors that are growing slowly can cause false-negative results.<sup>23,24</sup>

Consequently, more radiopharmaceuticals are needed to be employed in the clinical cancer management. We are focusing on designing and developing novel <sup>18</sup>F labeled radioactive tracers for PET imaging and we are especially interested in small molecular PET tracers for tumor detection. Although the anti-tumor activities and the corresponding mechanisms of pyrazolo[1,5-*a*]pyrimidines have been explored extensively, the application of <sup>18</sup>F labeled pyrazolo[1,5-*a*]pyrimidine derivatives in PET imaging has little been reported. Pyrazolo[1,5-*a*]pyrimidine core structure has several positions for introducing substituent, the C-5 position and the C-7 position were commonly used for introducing substituent in anti-tumor drug design.<sup>14,18,19,25,26</sup> As far as molecular design of radiopharmaceuticals is concerned, we should consider not only structural variety, but also radiochemical synthetic factors (which means faster synthesis of <sup>18</sup>F-labeled compound for production, a higher yield by avoiding side reactions and higher reproducibility). We previously explored a novel one-step <sup>18</sup>F fluorination synthetic method using 2,4-dinitrobenzoic acid modified targeting molecules as precursors.<sup>27</sup> This method was improved by us to modify the pyrazolo[1,5-*a*]pyrimidine and designed precursor **9** (Fig. 1). By labeling **9** with <sup>18</sup>F, we got [<sup>18</sup>F]**2** (Fig. 1). In addition, we also used tosylate as leaving group and designed precursor **7** (Fig. 1), which can be labeled with <sup>18</sup>F to get [<sup>18</sup>F]**1** (Fig. 1). The biological properties of these new radiotracers were evaluated in vitro and in vivo in comparison with [<sup>18</sup>F]FDG and L-[<sup>18</sup>F]FET.

The [<sup>19</sup>F]**1** and [<sup>19</sup>F]**2** were prepared from the same intermediate **5** which was synthesized from malonitrile through an easy four-step procedure (Scheme 1).<sup>26</sup>

The tosylate modified precursor **7** (Scheme 2) was prepared from intermediate **5** by the introducing of 4-methylbenzene-1-sulfonyl chloride bridged by 2-aminoethanol at C-7 position of pyrazolo[1,5-*a*]pyrimidine core structure, <sup>19</sup>F substitution [<sup>19</sup>F]**1** (Scheme 2) was obtained from precursor **7** using TBAF·3H<sub>2</sub>O in dry acetonitrile at 80 °C under nitrogen atmosphere for 5 h with 38% yield. The reaction is shown in Scheme 2.

The 2,4-dinitrobenzoic acid modified precursor **9** (Scheme 3) was prepared from intermediate **5** by the introducing of 2,4-dinitrobenzoic acid bridged by ethane-1,2-diamine at C-7 position of pyrazolo[1,5-*a*]pyrimidine core structure, <sup>19</sup>F substitution [<sup>19</sup>F]**2** was obtained from **9** using TBAF·3H<sub>2</sub>O in dry DMF at 120 °C for 40 min with 29% yield. The reaction is shown in Scheme 3.

The radiosynthesis of [<sup>18</sup>F]**1** and [<sup>18</sup>F]**2** was completed through a simple substitution (Scheme 4). [<sup>18</sup>F]**1** was obtained under a mild condition in dry acetonitrile refluxing under N<sub>2</sub> for 20 min with a

35% radiochemical yield (without decay correction). While [<sup>18</sup>F]**2** was prepared through a 25 min <sup>18</sup>F fluorination at 2'-nitryl in dry DMF under N<sub>2</sub> at 120 °C. The radiochemical yield was about 30% (without decay correction). Fixation of K[<sup>18</sup>F]F on Kryptofix 2.2.2. was used in both synthetic processes as <sup>18</sup>F fluidizer. The mixed product was highly diluted with water, adsorbed on a C18 Sep-Pak cartridge and almost quantitatively desorbed with acetonitrile. The crude products were purified by semi-preparative HPLC with reversed-phase Grace Alltima™ C18 Column (250×10 mm, particle size: 10 μm). The column was eluted with isocratic solvent system as follows: 30% water and 70% acetonitrile; flow rate: 5 L/min. The retention time of [<sup>18</sup>F]**1** was 3.061 min and the retention time of [<sup>18</sup>F]**2** was 3.160 min in our gradient, respectively. The desired product was collected from HPLC and the solvent was evaporated using a rotary evaporator. The product was dissolved in phosphate-buffered saline solution (pH 7.4). The nondecay-corrected radiochemical yields were approximately 30–35% and with specific activity between 41–50 GBq/μmol. The radiochemical purity and chemical purity were above 99%. The total reaction time for either [<sup>18</sup>F]**1** or [<sup>18</sup>F]**2** was about 60 min, with final high-performance liquid chromatography purification included.

The lipophilicity of both radiotracers was measured according to the method previously reported by us.<sup>27</sup> The partition coefficient (log *P*) values of [<sup>18</sup>F]**1** and [<sup>18</sup>F]**2** were 0.68 ± 0.02 and 0.69 ± 0.02, respectively. The similar partition coefficient of both radiotracers has demonstrated that the different substituents of [<sup>18</sup>F]**1** and [<sup>18</sup>F]**2** at C-7 position of pyrazolo[1,5-*a*]pyrimidine core structure did not lead to significant change in lipophilicity. The stability of each <sup>18</sup>F labeled compound in mouse plasma was determined by incubating 0.1 mL of [<sup>18</sup>F]**1** and [<sup>18</sup>F]**2** (3.7 MBq) in the solution of 0.5 mL murine plasma at 37 °C for 1 h and 2 h. Plasma proteins were precipitated by adding acetonitrile and removed by centrifugation. The supernatant part was injected into HPLC to determine the stability of each compound. The HPLC patterns indicated that both [<sup>18</sup>F]**1** and [<sup>18</sup>F]**2** were stable in mouse plasma.

Uptake kinetic of [<sup>18</sup>F]**1**, [<sup>18</sup>F]**2**, [<sup>18</sup>F]FDG and L-[<sup>18</sup>F]FET in S180 tumor cells<sup>28,29</sup> are shown in Figure 2. As shown, the uptake of [<sup>18</sup>F]**1** and [<sup>18</sup>F]FDG is rapid for the first 30 min, followed by a nearly steady state from 30 min onward. The maximum uptake of [<sup>18</sup>F]**1** is about two-fold of [<sup>18</sup>F]FDG. Radioactivity uptake into S180 tumor cells after a 60-min incubation at 37 °C (pH 7.4) varied from 9% to 23% of the total cell radioactivity uptake. On balance, a greater percentage of [<sup>18</sup>F]**1** relative to [<sup>18</sup>F]FDG was taken up into the cell at any given time. In comparison, the cell uptake of [<sup>18</sup>F]**2** and L-[<sup>18</sup>F]FET remained quantitatively low (<7%).

The biodistribution studies and tumor uptake were investigated in Kunming Mice bearing S180 tumor.<sup>30</sup> An approximately 370 kBq/0.1 mL phosphate-buffered saline solution (pH 7.4) of <sup>18</sup>F labeled compound purified by HPLC as described above was injected into the tail vein. The animals were sacrificed at 5 min, 15 min, 30 min, 60 min and 120 min post-injection. The tissues and organs of interest were immediately removed, weighed and measured for <sup>18</sup>F radioactivity in a γ counter. Values are expressed as mean ± SD (*n* = 4). The biodistribution data of [<sup>18</sup>F]**1** and [<sup>18</sup>F]**2** were summarized in Table 1 and Table 2 above, respectively. All the animal studies were carried out in compliance with relevant national laws relating to the conduct of animal experimentation.

Table 1 showed the biodistribution of [<sup>18</sup>F]**1**. After a fast distribution, [<sup>18</sup>F]**1** was excreted from the body mainly through the kidney. Radioactivity of [<sup>18</sup>F]**1** in tumor was 1.88 ± 0.63, 4.37 ± 0.30, 5.51 ± 0.31, 2.95 ± 0.36 and 2.88 ± 0.34 ID/g at 5 min, 15 min, 30 min, 60 min, and 120 min post-injection, respectively, a remarkable increasing uptake of this compound in tumor. Meanwhile, radioactivity of [<sup>18</sup>F]**1** in other organs and tissues decreased rapidly. The tumor/brain, tumor/muscle and tumor/blood ratios reached high levels of 2.23, 1.81 and 1.23 at 30 min post-injection.

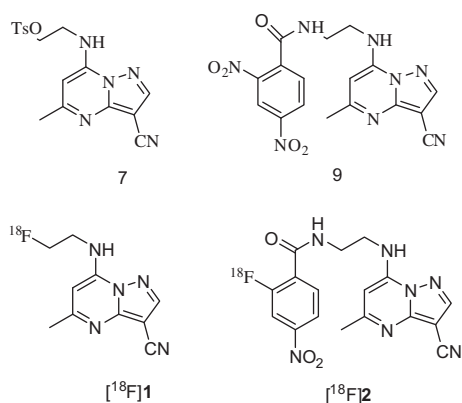
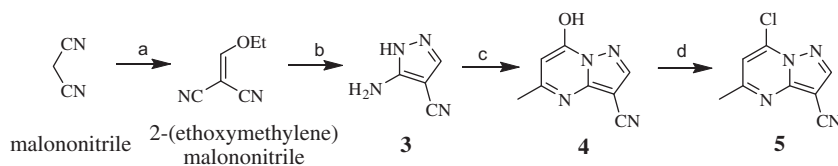
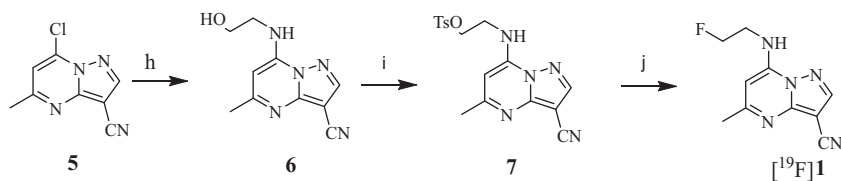


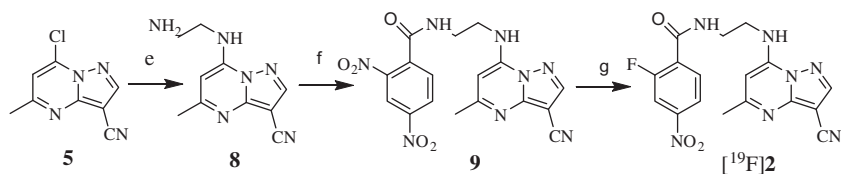
**Figure 1.** Structure of <sup>18</sup>F labeled pyrazolo[1,5-*a*]pyrimidine derivatives and their corresponding precursors.



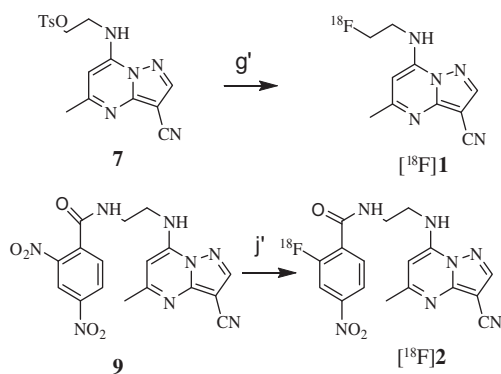
**Scheme 1.** Synthesis of intermediate **5**. Experiment reagents and conditions: (a)  $\text{HC}(\text{OC}_2\text{H}_5)_3$ ,  $\text{Ac}_2\text{O}$ , refluxing, 6 h, then  $0^\circ\text{C}$ , 12 h, 84%; (b) 85%  $\text{H}_2\text{NNH}_2\cdot\text{H}_2\text{O}$ ,  $100^\circ\text{C}$ , 1 h, then 10 mL  $\text{H}_2\text{O}$ ,  $0^\circ\text{C}$ , 12 h, 81%; (c)  $\text{CH}_3\text{COCH}_2\text{COOCH}_2\text{CH}_3$ ,  $\text{AcOH}$ , refluxing 4 h, 78%; (d)  $\text{POCl}_3$ ,  $\text{Py}$ , stirred at  $85^\circ\text{C}$ ,  $120^\circ\text{C}$ , 1 h, then added  $\text{CHCl}_3$  at  $60^\circ\text{C}$ , refluxing 1 h, followed by adding water at  $0^\circ\text{C}$ , 87%.



**Scheme 2.** Synthesis of  $[^{19}\text{F}]\mathbf{1}$ . Experiment reagents and conditions: (h)  $\text{HOCH}_2\text{CH}_2\text{NH}_2$ ,  $\text{CH}_3\text{CH}_2\text{OH}$ , refluxing 4 h, 54%; (i)  $\text{TsCl}$ ,  $\text{TEA}$ ,  $\text{DMAP}$ ,  $\text{CH}_2\text{Cl}_2$ ,  $0^\circ\text{C}$ , 0.5 h, then rt, 12 h, 45%; (j)  $\text{TBAF}\cdot 3\text{H}_2\text{O}$ ,  $\text{CH}_3\text{CN}$ ,  $\text{N}_2$ , refluxing 5 h, 38%.



**Scheme 3.** Synthesis of  $[^{19}\text{F}]\mathbf{2}$ . Experiment reagents and conditions: (e)  $\text{H}_2\text{NCH}_2\text{CH}_2\text{NH}_2$ ,  $\text{CH}_3\text{CH}_2\text{OH}$ , refluxing 4 h, 81%; (f) 2,4-dinitrobenzoic acid,  $\text{TEA}$ ,  $\text{HOBT}$ ,  $\text{DCC}$ ,  $\text{CH}_2\text{Cl}_2$ ,  $0^\circ\text{C}$ , 0.5 h, then rt, 12 h, 51%; (g)  $\text{TBAF}\cdot 3\text{H}_2\text{O}$ ,  $\text{DMF}$ ,  $120^\circ\text{C}$ , 40 min, 29%.



**Scheme 4.** Radiochemical synthesis of  $[^{18}\text{F}]\mathbf{1}$  and  $[^{18}\text{F}]\mathbf{2}$ . Experiment reagents and conditions: (g')  $\text{K } [^{18}\text{F}] \text{F}$ , Kryptofix 2.2.2.,  $\text{CH}_3\text{CN}$ ,  $80^\circ\text{C}$ , 20 min, 35%; (j')  $\text{K } [^{18}\text{F}] \text{F}$ , Kryptofix 2.2.2.,  $\text{DMF}$ ,  $120^\circ\text{C}$ , 25 min, 30%.

Table 2 showed a rapid distribution of  $[^{18}\text{F}]\mathbf{2}$  into all organs and tissues after injection. Radioactivity uptake in all organs and tissues reached their peak values at the initial time and then sharp decline occurred as time elapsed. The relatively low uptake of  $[^{18}\text{F}]\mathbf{2}$  in brain which decreased through the course of study from  $0.38 \pm 0.07\text{ID/g}$  at 5 min pi. to  $0.04 \pm 0.00\text{ID/g}$  at 120 min pi. gave the high tumor/brain ratios: 5.87, 12.35, 10.44, 8.69 and 5.13 at 5 min, 15 min, 30 min, 60 min and 120 min, respectively. Moreover, the tumor had a proportion of  $2.26 \pm 0.48\text{ID/g}$  at 5 min pi., not preponderating over other organs or tissues. However, as a result of a relatively slower elimination in tumor, both the tumor/muscle and tumor/blood ratios of  $[^{18}\text{F}]\mathbf{2}$  had a continual increasing for a long time post-injection, and reached their maximum 1.57 and 2.50 at 60 min and 120 min, respectively.

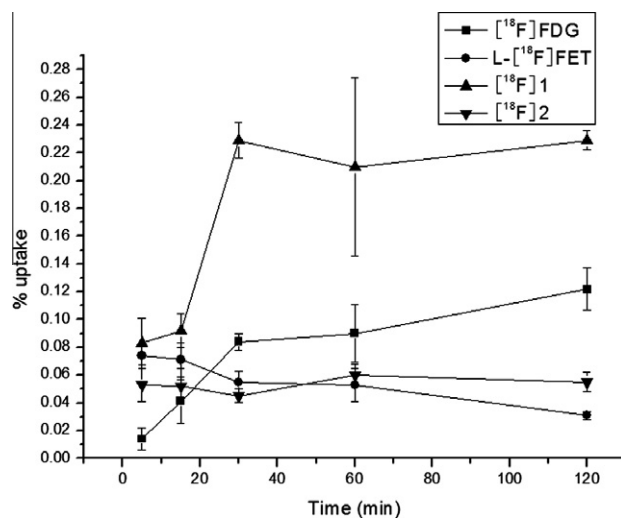


**Figure 2.** Uptake kinetics of  $[^{18}\text{F}]\text{FDG}$ , L- $[^{18}\text{F}]\text{FET}$ ,  $[^{18}\text{F}]\mathbf{1}$  and  $[^{18}\text{F}]\mathbf{2}$  into S180 tumor cells at  $37^\circ\text{C}$  (pH 7.4).

Comparing the biodistribution data of  $[^{18}\text{F}]\mathbf{1}$  and  $[^{18}\text{F}]\mathbf{2}$  in mice bearing S180 tumor as shown in Table 1 and Table 2, there were significant differences in initial uptake, accumulation and clearance in brain and tumor. Meanwhile, we noticed that  $[^{18}\text{F}]\mathbf{1}$  and  $[^{18}\text{F}]\mathbf{2}$  had a similar lipophilicity, as it was characterized by both the much close  $\log P$  values ( $0.69 \pm 0.02$  for  $[^{18}\text{F}]\mathbf{1}$  and  $0.68 \pm 0.02$  for  $[^{18}\text{F}]\mathbf{2}$ ) and retention time (3.061 min for  $[^{18}\text{F}]\mathbf{1}$  and 3.160 min for  $[^{18}\text{F}]\mathbf{2}$ ) on the same analytical HPLC system. Therefore, the ability to penetrate BBB (blood–brain barrier) for both radioactivity tracers is supposed to be comparable. However, the brain uptake of  $[^{18}\text{F}]\mathbf{1}$  is much higher than that of  $[^{18}\text{F}]\mathbf{2}$ :  $3.17 \pm 0.48$ ,

**Table 1**  
Biodistribution of [<sup>18</sup>F]1 in mice bearing S180 tumor. Expressed as% injected dose per gram (% ID/g ± SD), n = 4

Organs	Time (min)				
	5	15	30	60	120
Heart	5.53 ± 0.61	3.57 ± 0.65	4.06 ± 0.09	3.46 ± 0.78	2.59 ± 0.18
Liver	6.99 ± 1.00	4.02 ± 0.20	3.17 ± 0.16	2.45 ± 0.30	1.84 ± 0.22
Spleen	4.66 ± 0.26	3.42 ± 0.52	3.43 ± 0.39	2.82 ± 0.31	2.15 ± 0.94
Lung	6.61 ± 0.54	3.79 ± 0.93	3.77 ± 0.31	2.78 ± 0.19	2.54 ± 0.96
Kidney	7.93 ± 1.27	5.04 ± 0.48	3.28 ± 0.20	2.58 ± 0.16	1.92 ± 0.40
Brain	3.17 ± 0.48	2.70 ± 0.07	2.47 ± 0.24	1.93 ± 0.25	1.79 ± 0.27
Muscle	3.99 ± 1.05	3.84 ± 0.45	3.05 ± 0.22	2.31 ± 0.48	2.64 ± 0.60
Blood	4.83 ± 0.45	4.65 ± 0.05	4.49 ± 0.31	3.63 ± 0.33	2.95 ± 0.30
Tumor	1.88 ± 0.63	4.37 ± 0.30	5.51 ± 0.31	2.95 ± 0.36	2.88 ± 0.34
Tumor/brain	0.59	1.62	2.23	1.53	1.61
Tumor/muscle	0.47	1.14	1.81	1.28	1.09
Tumor/blood	0.39	0.94	1.23	0.81	0.98

**Table 2**  
Biodistribution of [<sup>18</sup>F]2 in mice bearing S180 tumor. Expressed as% injected dose per gram (% ID/g ± SD), n = 4

Organs	Time (min)				
	5	15	30	60	120
Heart	5.77 ± 0.77	2.78 ± 0.16	1.16 ± 0.23	0.63 ± 0.01	0.12 ± 0.02
Liver	17.90 ± 1.70	10.12 ± 0.34	7.30 ± 1.06	4.07 ± 0.60	2.05 ± 0.17
Spleen	4.54 ± 0.86	1.96 ± 0.25	0.99 ± 0.24	0.53 ± 0.08	0.14 ± 0.03
Lung	5.60 ± 0.66	2.60 ± 0.24	1.19 ± 0.08	0.56 ± 0.26	0.19 ± 0.07
Kidney	17.70 ± 1.04	8.45 ± 0.35	5.63 ± 0.58	1.83 ± 0.50	0.74 ± 0.03
Brain	0.38 ± 0.07	0.16 ± 0.01	0.12 ± 0.02	0.08 ± 0.02	0.04 ± 0.00
Muscle	3.82 ± 0.39	2.07 ± 0.83	0.89 ± 0.17	0.47 ± 0.16	0.28 ± 0.07
Blood	5.23 ± 0.16	2.50 ± 0.37	1.42 ± 0.43	0.45 ± 0.12	0.09 ± 0.04
Tumor	2.26 ± 0.48	1.99 ± 0.21	1.24 ± 0.39	0.74 ± 0.12	0.21 ± 0.02
Tumor/brain	5.87	12.35	10.44	8.69	5.13
Tumor/muscle	0.59	0.96	1.40	1.57	0.77
Tumor/blood	0.43	0.80	0.88	1.66	2.50

2.70 ± 0.07, 2.47 ± 0.24, 1.93 ± 0.25 and 1.79 ± 0.27%ID/g for [<sup>18</sup>F]1 and 0.38 ± 0.07, 0.16 ± 0.01, 0.12 ± 0.02, 0.08 ± 0.02 and 0.04 ± 0.00%ID/g for [<sup>18</sup>F]2 at 5 min, 15 min, 30 min, 60 min and 120 min post-injection. It was reported that the ideal log *P* value for molecules to penetrate the BBB is between 1 and 3.<sup>31</sup> The log *P* values of both radioactivity tracers are less than 1, thus it is reasonable for the low brain uptake for [<sup>18</sup>F]2, whereas, it could not explain the high uptake of [<sup>18</sup>F]1 in brain. In addition, as the time lapsed, the tumor uptake of [<sup>18</sup>F]1 and [<sup>18</sup>F]2 behaved differently: [<sup>18</sup>F]1 reached its peak of 5.51 ± 0.31%ID/g at 30 min pi. and then decreased to 2.88 ± 0.34%ID/g at 120 min post-injection, 52% radioactivity still retained in the body after 120 min indicating good persistence in tumor uptake. On the other hand, [<sup>18</sup>F]2 had a relative high initial tumor uptake 2.26 ± 0.48%ID/g at 5 min but the rate of elimination from tumor was rapid with only 0.21 ± 0.02%ID/g at 120 min post-injection. From the uptake results, we could make some inference that the distribution of [<sup>18</sup>F]1 underwent a special transport mechanism and apparently much more suitable for PET tumor imaging.

In order to confirm this, we compared [<sup>18</sup>F]FDG and L-[<sup>18</sup>F]FET with [<sup>18</sup>F]1 in the same animal model, the results were shown in Table 3.

As shown in Table 3, [<sup>18</sup>F]FDG had high tumor/blood ratios after 30 min post-injection due to fast clearance from the blood. The tumor/blood ratios were 11.38, 19.47 and 15.85 after 30 min, 60 min and 120 min post-injection, respectively. The high uptake in brain resulted in low tumor/brain ratios. The maximum value of tumor/brain ratio was 1.33 at 120 min post-injection. Therefore, [<sup>18</sup>F]FDG is not an ideal PET imaging agent for brain tumors. As show in Table 3, in contrast to [<sup>18</sup>F]FDG, L-[<sup>18</sup>F]FET had much lower

tumor/blood ratios. However, it had higher tumor/brain ratios (the maximum value was 2.95 at 120 min pi.), which was suitable for the application in PET imaging agent of brain tumors and made it a necessary complement to [<sup>18</sup>F]FDG.

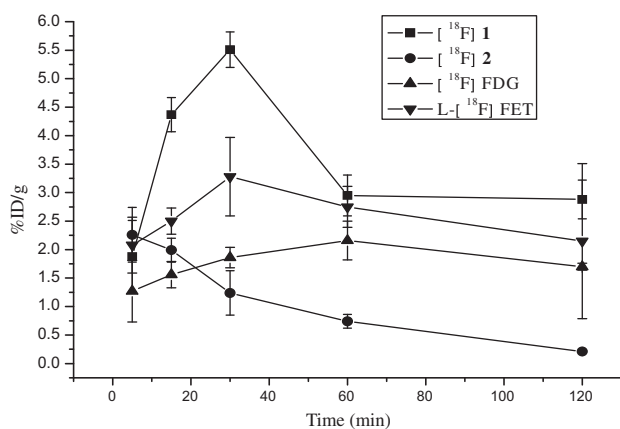
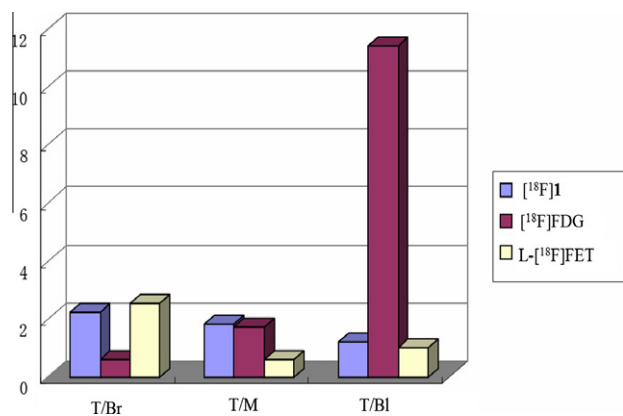
By comparison with [<sup>18</sup>F]FDG and L-[<sup>18</sup>F]FET, [<sup>18</sup>F]1 displayed some peculiarities: [<sup>18</sup>F]1 had significantly higher absolute radioactivity uptake in tumor than those of [<sup>18</sup>F]FDG and L-[<sup>18</sup>F]FET at all time points as shown in Figure 3. The maximum uptake of [<sup>18</sup>F]1 in tumor was 5.51 ± 0.31%ID/g, nearly three times as much as that of [<sup>18</sup>F]FDG and two times as much as that of L-[<sup>18</sup>F]FET at 30 min post-injection.

At the same time (30 min post-injection), as shown in Figure 4, the tumor to brain ratio reached the peak 2.23 which was similar to that of L-[<sup>18</sup>F]FET (2.54) and much higher than that of [<sup>18</sup>F]FDG (0.61); the tumor to muscle ratio was 1.81 which was similar to that of [<sup>18</sup>F]FDG (1.75) and much higher than that of L-[<sup>18</sup>F]FET (0.62); the tumor to blood ratio also reached the maximum of 1.23, slightly higher than that of L-[<sup>18</sup>F]FET (1.03). Taken together, [<sup>18</sup>F]1 had the capability to accumulate in tumor and could greatly enhance the sensitivity in tumor imaging. As a radioactivity tracer, [<sup>18</sup>F]1 may be useful for PET imaging of both central and peripheral tumors as well as metastasis of tumors.

In order to visualize the distribution of [<sup>18</sup>F]1, small animal PET imaging studies was performed in the mouse bearing S180 tumor. The mouse was injected intravenously with approximately 3.7 MBq of [<sup>18</sup>F]1 in saline and anesthetized with 1.5% isoflurane for imaging. Whole body image was acquired by micro PET at 30 min post-injection is shown in Figure 5. As expected from the ex vivo biodistribution data, tracer uptake in excretory organs was predominant, but tumor (pointed to by the arrowhead) in

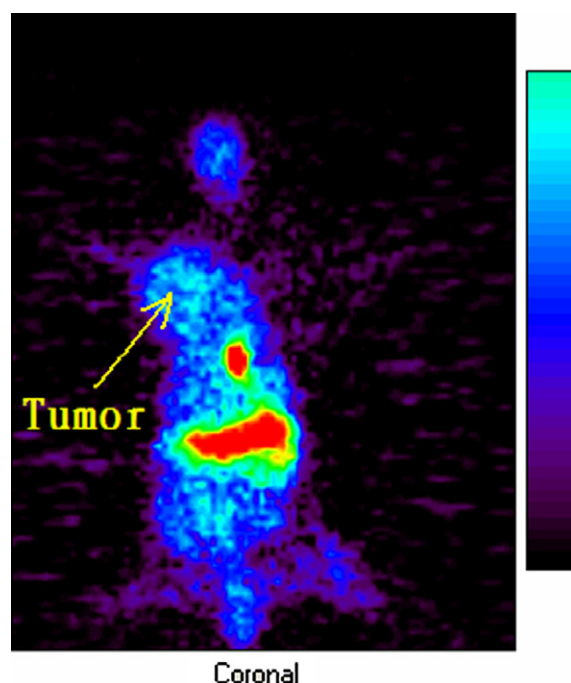
**Table 3**The biodistribution comparison of [ $^{18}\text{F}$ ] **1**, [ $^{18}\text{F}$ ]FDG and L-[ $^{18}\text{F}$ ]FET in mice bearing S180 tumor. Expressed as% injected dose per gram (% ID/g  $\pm$  SD),  $n = 4^a$ 

Organs	Compounds	Time (min)				
		5	15	30	60	120
Tumor	[ $^{18}\text{F}$ ] <b>1</b>	1.88 $\pm$ 0.63	4.37 $\pm$ 0.30	5.51 $\pm$ 0.31	2.95 $\pm$ 0.36	2.88 $\pm$ 0.34
	[ $^{18}\text{F}$ ]FDG	1.27 $\pm$ 0.54	1.56 $\pm$ 0.23	1.86 $\pm$ 0.18	2.16 $\pm$ 0.34	1.70 $\pm$ 0.06
	L-[ $^{18}\text{F}$ ]FET	2.08 $\pm$ 0.49	2.50 $\pm$ 0.23	3.28 $\pm$ 0.69	2.75 $\pm$ 0.36	2.15 $\pm$ 1.36
Tumor/brain	[ $^{18}\text{F}$ ] <b>1</b>	0.59	1.62	2.23	1.53	1.61
	[ $^{18}\text{F}$ ]FDG	0.53	0.59	0.61	1.02	1.33
	L-[ $^{18}\text{F}$ ]FET	2.10	2.43	2.54	2.93	2.95
Tumor/muscle	[ $^{18}\text{F}$ ] <b>1</b>	0.47	1.14	1.81	1.28	1.09
	[ $^{18}\text{F}$ ]FDG	0.81	1.37	1.75	2.23	2.20
	L-[ $^{18}\text{F}$ ]FET	0.72	0.75	0.62	1.23	1.04
Tumor/blood	[ $^{18}\text{F}$ ] <b>1</b>	0.39	0.94	1.23	0.81	0.98
	[ $^{18}\text{F}$ ]FDG	1.17	3.42	11.38	19.47	15.85
	L-[ $^{18}\text{F}$ ]FET	0.31	0.76	1.02	1.10	1.92

<sup>a</sup> The data of [ $^{18}\text{F}$ ]FDG and L-[ $^{18}\text{F}$ ]FET were quoted from Ref. 27.**Figure 3.** Comparison of tumor uptake rates of [ $^{18}\text{F}$ ]**1** and [ $^{18}\text{F}$ ]**2** with those of [ $^{18}\text{F}$ ]FDG and L-[ $^{18}\text{F}$ ]FET in the same animal model bearing S180 tumor.**Figure 4.** Comparison of tumor to brain (T/Br), tumor to muscle (T/M) and tumor to blood (T/B) uptake ratios of [ $^{18}\text{F}$ ]**1** with those of [ $^{18}\text{F}$ ]FDG and L-[ $^{18}\text{F}$ ]FET at 30 min post-injection in the same animal model bearing S180 tumor.

the left forelimb was also obvious, while no accumulation in the right forelimb was found. The imaging results clearly confirmed [ $^{18}\text{F}$ ]**1** could be accumulated in tumor.

In conclusion, we successfully labeled pyrazolo[1,5-*a*]pyrimidine derivatives by two time-saving and high-yield methods and got two novel  $^{18}\text{F}$  labeled compounds, [ $^{18}\text{F}$ ]**1** and [ $^{18}\text{F}$ ]**2**. The in vitro studies showed a high uptake of [ $^{18}\text{F}$ ]**1** by the S180 tumor

**Figure 5.** Coronal PET image of Kunming mice with S180 tumor (arrow) in the left front flank at 30 min post-injection of [ $^{18}\text{F}$ ]**1**.

cells. Preliminary biodistribution experiments were performed in S180 tumor-bearing mice to evaluate the potential of [ $^{18}\text{F}$ ]**1** and [ $^{18}\text{F}$ ]**2** for application in PET tumor imaging. The comparative in ex vivo analysis of [ $^{18}\text{F}$ ]**1**, [ $^{18}\text{F}$ ]**2**, [ $^{18}\text{F}$ ]FDG and L-[ $^{18}\text{F}$ ]FET showed superior characteristics for [ $^{18}\text{F}$ ]**1** with respect to the total tracer accumulation and retention in tumor. PET imaging revealed that the accumulation of radioactivity in S180 tumor was visualized. The positive in vitro and in vivo results of [ $^{18}\text{F}$ ]**1** suggest that this compound represents a promising PET tracer candidate for tumor detection. On the other hand, on-going effort to optimize the structure of [ $^{18}\text{F}$ ]**1** aiming at enhancing the tumor-to-nontarget ratios in vivo is under way.

#### Acknowledgments

This project was sponsored by the National Natural Science foundation of China (No. 21071022). We also thank the cyclotron operator team of the PET Centre of Xuanwu Hospital for providing fluoride-18 nuclide and technical assistance.

## Supplementary data

Supplementary data associated with this article can be found, in the online version, at doi:10.1016/j.bmcl.2011.06.072.

## References and notes

- George, C. F. P. *Lancet* **2001**, 357, 1623.
- Stefano, A.; Anna, A.; Maurizio, B.; Alessandra, T.; Francisco, O.; Francesco, O.; Silvia, S.; Chiara, B.; Matilde, Y. *ChemMedChem* **2010**, 5, 1242.
- Curran, K. J.; Verheijen, J. C.; Kaplan, J.; Richard, D. J.; Toral-Barza, L.; Hollander, I.; Lucas, J.; Ayrál-Kaloustian, S.; Yu, K.; Zask, A. *Bioorg. Med. Chem. Lett.* **2010**, 20, 1440.
- Zask, A.; Verheijen, J. C.; Curran, K.; Kaplan, J.; Richard, D. J.; Nowak, P.; Malwitz, D. J.; Brooijmans, N.; Bard, J.; Svenson, K.; Lucas, J.; Toral-Barza, L.; Zhang, W.-G.; Hollander, I.; Gibbons, J. J.; Abraham, R. T.; Ayrál-Kaloustian, S.; Mansour, T. S.; Yu, K. *J. Med. Chem.* **2009**, 52, 5013.
- Manetti, F.; Santucci, A.; Locatelli, G. A.; Maga, G.; Spreafico, A.; Serchi, T.; Orlandini, M.; Bernardini, G.; Caradonna, N. P.; Spallarossa, A.; Brullo, C.; Schenone, S.; Bruno, O.; Ranise, A.; Bondavalli, F.; Hoffmann, O.; Bologna, M.; Angelucci, A.; Botta, M. *J. Med. Chem.* **2007**, 50, 5579.
- Schenone, S.; Bruno, O.; Ranise, A.; Bondavalli, F.; Brullo, C.; Fossa, P.; Mosti, L.; Menozzi, G.; Carraro, F.; Naldini, A.; Bernini, C.; Manetti, F.; Botta, M. *Bioorg. Med. Chem. Lett.* **2004**, 14, 2511.
- Traxler, P.; Bold, G.; Frei, J.; Lang, M.; Lydon, N.; Mett, H.; Buchdunger, E.; Meyer, T.; Mueller, M.; Furet, P. *J. Med. Chem.* **1997**, 40, 3601.
- Ballell, L.; Field, R. A.; Chungc, G. A. C.; Youngc, R. J. *Bioorg. Med. Chem. Lett.* **2007**, 17, 1736.
- Gudmundsson, K. S.; Johns, B. A.; Weatherhead, J. *Bioorg. Med. Chem. Lett.* **2009**, 19, 5689.
- Rashad, A. E.; Hegab, M. I.; Abdel-Megeid, R. E.; Micky, J. A.; Abdel-Megeid, F. M. *E. Bioorg. Med. Chem.* **2008**, 16, 7102.
- Frizzo, C. P.; Scapin, E.; Campos, P. T.; Moreira, D. N.; Martins, M. A. P. *J. Mol. Struct.* **2009**, 933, 142.
- Novinson, T.; Bhooshan, B.; Okabe, T.; Revankar, G. R.; Wilson, H. R.; Robins, R. K.; Senga, K. *J. Med. Chem.* **1976**, 19, 512.
- Senga, K.; Novinson, T.; Wilson, H. R.; Robins, R. K. *J. Med. Chem.* **1981**, 24, 610.
- Di Grandi, M. J.; Berger, D. M.; Hopper, D. W.; Zhang, C.; Dutia, M.; Dunnick, A. L.; Torres, N.; Levin, J. I.; Diamantidis, G.; Zapf, C. W.; Bloom, J. D.; Dennis Powell, Y. B. H.; Wojciechowicz, D.; Collins, K.; Frommer, E. *Bioorg. Med. Chem. Lett.* **2009**, 19, 6957.
- Ahmeda, O. M.; Mohamedc, M. A.; Ahmedb, R. R.; Ahmedd, S. A. *Eur. J. Med. Chem.* **2009**, 44, 3519.
- Heathcote, D. A.; Patel, H.; Kroll, S. H. B.; Hazel, P.; Periyasamy, M.; Alikian, M.; Kanneganti, S. K.; Jogalekar, A. S.; Scheiper, B.; Barbazanges, M.; Blum, A.; Brackow, J.; Siwicka, A.; Pace, R. D. M.; Fuchter, M. J.; Snyder, J. P.; Liotta, D. C.; Freemont, P. S.; Aboagye, E. O.; Coombes, R. C.; Barrett, A. G. M.; Ali, S. J. *Med. Chem.* **2010**, 53, 8508.
- Fraley, M. E.; Rubino, R. S.; Hoffman, W. F.; Hambaugh, S. R.; Arrington, K. L.; Hungate, R. W.; Bilodeau, M. T.; Tebben, A. J.; Rutledge, R. Z.; Kendall, R. L.; McFall, R. C.; Huckle, W. R.; Coll, K. E.; Thomas, K. A. *Bioorg. Med. Chem. Lett.* **2002**, 12, 3537.
- Powell, D.; Gopalsamy, A.; Wang, Y. D.; Zhang, N.; Miranda, M.; McGinnisb, J. P.; Rabindranb, S. K. *Bioorg. Med. Chem. Lett.* **2007**, 17, 1641.
- Gopalsamy, A.; Yang, H.; Ellingboe, J. W.; Tsou, H.-R.; Zhang, N.; Honores, E.; Powell, D.; Miranda, M.; McGinnisb, J. P.; Rabindranb, S. K. *Bioorg. Med. Chem. Lett.* **2005**, 15, 1591.
- Koehler, L.; Graf, F.; Bergmann, R.; Steinbach, J.; Pietzsch, J.; Wuest, F. *Eur. J. Med. Chem.* **2010**, 45, 727.
- Miller, P. W.; Long, N. J.; Vilar, R.; Gee, A. D. *Angew. Chem., Int. Ed.* **2008**, 47, 8998.
- Varagnolo, L.; Stokkel, M. P. M.; Mazzi, U.; Pauwels, E. K. J. *Nucl. Med. Biol.* **2000**, 27, 103.
- Yu, W.; McConathy, J.; Williams, L.; Camp, V. M.; Malveaux, E. J.; Zhang, Z.; Olson, J. J.; Goodman, M. M. *J. Med. Chem.* **2010**, 53, 876.
- Wood, K. A.; Hoskin, P. J.; Saunders, M. I. *Clin. Oncol.* **2007**, 19, 237.
- Gopalsamy, A.; Ciszewski, G.; Hu, Y.; Lee, F.; Feldberg, L.; Frommer, E.; Kim, S.; Collins, K.; Wojciechowicz, D.; Mallon, R. *Bioorg. Med. Chem. Lett.* **2009**, 19, 2735.
- Li, J.; Zhao, Y.; Zhao, X.; Yuan, X.; Gong, P. *Arch. Pharm. Chem. Life Sci.* **2006**, 339, 593.
- Qiao, Y.; He, Y.; Zhang, S.; Li, G.; Liu, H.; Xu, J.; Wang, X.; Qi, C.; Peng, C. *Bioorg. Med. Chem. Lett.* **2009**, 19, 4873.
- Sun, X.; Chu, T.; Wang, X. *Nucl. Med. Biol.* **2010**, 37, 117.
- S180 tumor cells were suspended in fresh DMEM medium supplemented with 10% fetal bovine serum at a cell concentration of  $2 \times 10^6$  cells/mL. Aliquots of 10 mL were placed in glass vials and incubated at 37 °C with gentle stirring under an atmosphere of 95% air plus 5% carbon dioxide. After a 30- to 45-min equilibration period, 0.15 mL of cell culture medium with about 0.25 MBq/mL radiotracer was added and incubated at 37 °C. At 5, 15, 30, 60 and 120 min, 200  $\mu$ L samples of the suspension were transferred to microfuge tubes and centrifuged at 1500 rpm for 5 min. A 180- $\mu$ L sample of each supernatant was removed for counting, and the left sample containing cells and 20  $\mu$ L medium was also counted. Percent cell uptake is calculated as  $[\text{residue counts} - (\text{supernatant counts}/9)]/(\text{residue counts} + \text{supernatant counts}) \times 100\%$ . The data are expressed as mean  $\pm$  S.D. ( $n = 5$ ). During all the experiments, cell viability was always greater than 90%.
- The S180 tumor model was established by injecting subcutaneously  $5 \times 10^6$  tumor cells into the left forelimb of Kunming mice weighing  $18 \pm 2$  g on average, the biodistribution studies were performed after the tumor cells were inoculated for 7–14 days when the tumors were 0.5–0.8 cm in diameter.
- Evensa, N.; Muccioli, G. G.; Houbrechtsa, N.; Lambertb, D. M.; Verbruggena, A. M.; Laerec, K. V.; Bormansa, G. M. *Nucl. Med. Biol.* **2009**, 36, 455.